

Zinc Oxide Nanostructures of Controlled Morphology Prepared from Single Source Precursors by Wet Chemical Route

¹Hameed Ullah*, ¹Javid Khan, ²Habib Nasir, ³Asad Muhammad Khan, ¹Mohsan Nawaz
¹Masroor Ahmad Bangesh and ¹Muhammad Irfan

¹Department of Chemistry, Hazara University Mansehra, Pakistan.

²School of Chemical and Materials Engineering, National University Science and Technology
Islamabad, Pakistan.

³Department of Chemistry, COMSATS Institute of Information Technology, Abbottabad, Pakistan.
hameedwazir@yahoo.co.uk*

(Received on 30th May 2016, accepted in revised form 4th May 2017)

Summary: Controlled and reproducible synthesis of ZnO nanoparticles with uniform size and shape is highly desirable for tuning its physico-chemical properties. Metal β -diketonates have many advantages as precursors in sol gel process over the conventional metal salts. Exploiting the advantageous characteristics of Zn(tmhd)₂ (where tmhd = 2,2,6,6-tetramethylheptane-3,5-dionate), we have synthesized ZnO nanoparticles by wet chemical (sol gel) method in acidic (pH 3) and basic (pH 9) media, and subsequently annealed at 250°C and 550°C. The resulting particles exhibited Wurtzite (hexagonal) crystal structure. The variation in pH and temperature has shown appreciable impact on the crystallite size and the morphology of the final product. The increase in particle size with increasing sintering temperature was reflected in the band gap energy, IR spectra and surface area measurements. Cylindrical, rod like nanoparticles were obtained at acidic pH 3 while spherical particles were achieved at basic pH 9 when sintered at 250°C. However, the particles obtained at sintering temperature of 250°C and 550°C were morphologically different. The lower pH 3 particles have elongated and flat shapes, while the higher pH 9 have hexagonal rod like particles when sintered at 550°C.

Keywords: Single Source Precursor; Zinc Oxide; Wet Chemistry; pH; Morphology.

Introduction

The last couple of decades have seen a tremendous growth in the field of nanomaterials-synthesis, characterization, and applications. The conventional materials are now studied under the domain of nanoscience which led to the emergence of nanotechnology. The impact of particle size below 100 nm upon the physical and chemical properties of materials and devices is now an accepted fact. The physico-chemical properties vary significantly with the changing particle size in the nano domain (<100 nm) [1-2]. The transformation of particle size from bulk to nano introduces novel chemical, physical, mechanical, magnetic and optical properties in the resulting materials [3]. The direct bandgap semiconductors metal oxides (MOs) are no exception to the effect of nano sized structures upon the characteristics of these materials. Zinc oxide (ZnO) is one of the MOs having wide direct band gap energy (E_g) of 3.37 eV and higher exciton binding energy of 60 meV at room temperature [4]. The unprecedented characteristics of ZnO having particles size in nanometer level scale is evident from the fact that ZnO nanomaterial is now widely used in UV filters and in the pharmaceutical and cosmetic products as bactericide [5, 6]. In addition, ZnO nanomaterials are also extensively used in the fabrication of many devices including photo-detectors, surface acoustic

wave devices, UV nano-lasers, solar cells, gas sensors, biosensors, ceramics, field emission, and nanogenerators [7-15].

The characteristics of ZnO nanomaterials are highly dependent upon the homogeneity and uniformity in particle size, shape, and morphology. Therefore, ZnO nanomaterials with desired properties could only be obtained for practical purposes if a strict control over the nanostructure is achieved. Many preparatory methods have been applied previously to get ZnO nanomaterials with desired characteristics [16, 17]. Among them, sol gel is used extensively for the synthesis of ZnO nanomaterials due to low energy requirements and economical feasibility. The microstructure of the resulting ZnO produced by sol gel method varies significantly with the nature of the precursors [18]. Therefore, the role of precursor in sol gel is vital for obtaining ZnO of the desired microstructure and characteristics. Metal salts (nitrates, chlorides, and perchlorates) are attractive precursors owing to their low cost, facilitative use and commercial availability, and have been used widely for the synthesis of ZnO nanomaterials by sol gel [19, 20]. However, the difficulty in exclusion and/or removal of the anionic species from the resulting nanoparticles is the serious

*To whom all correspondence should be addressed.

drawback of the use of salts as precursors. Zinc alkoxides are also interesting precursors because of their fast hydrolyzing nature. However, the lack of control over the hydrolysis process limits the chances of getting ZnO nanomaterials of homogeneous and uniform particle size and shape. Zinc Acetate is common precursor for the sol gel synthesis of ZnO nanostructures [21, 22]. The advantages of the precursor are moderate hydrolysis rate allowing control over the process and working of acetate group as stabilizer giving ZnO nanoparticles of homogenous and uniform microstructure [23].

Due to their volatility and vapor phase stability, the metal β -diketonates have attracted attention as precursors for metal organic chemical vapor deposition (MOCVD) [24]. However, the hydrated zinc acetyl acetonate ($\text{Zn}(\text{acac})_2 \cdot \text{H}_2\text{O}$) has also been used as precursor in sol gel for the synthesis of ZnO nanoparticles [25]. It has been observed that the microstructure of the resulting ZnO nanomaterials depends upon different variables.

Here we report the synthesis of ZnO nanomaterials by sol gel method employing bis(2,2,6,6-tetramethylheptane-3,5-dione)zinc(II) ($\text{Zn}(\text{tmhd})_2$) as precursor while NaOH and HCl as reagent for adjusting the pH of the media. The possibility of stabilizing ZnO nanoparticles with the help of tmhd has been exploited for obtaining ZnO nanomaterials having homogeneity and uniformity in the particle size and shape. The effect of pH upon the crystallite and particle size, and particle shape has been studied along with the effect of sintering temperature. Although the $\text{Zn}(\text{tmhd})_2$ have been previously reported for the deposition of ZnO and ZnS thin films by MOCVD technique [26, 27], but to the best of our knowledge the precursor is not used for the preparation of ZnO nanostructures by sol gel method.

Experimental

Materials and Methods

The chemicals used in this project were purchased from commercial suppliers. Zinc acetate ($\text{Zn}(\text{OAc})_2$) and 2,2,6,6-tetramethylheptane-3,5-dione (tmhdH) are from Sigma-Aldrich, and Sodium hydroxide (NaOH) from MERK, were used as received without any further purifications. The ethanol (Et_2OH) was dried by refluxing from sodium (Na) wires and stored over Na wires under dried gaseous nitrogen (N_2).

The Fourier Transform Infrared Spectra (FT-IR) were recorded in solid state using IR spectrometer (Nicolet 6700 from Thermo Scientific Company) in ATR mode. The UV-Visible spectra were obtained using Shimadzu (Model Pharma Spec UV-1700) spectrophotometer. XPert PRO Diffractometer equipped with Cu-K α radiations ($\lambda = 1.54 \text{ \AA}$) was used for measuring the X-rays Diffraction (XRD) patterns of the ZnO nanomaterials. Scanning Electron Microscope (SEM) (JEOLmodelJSM-6490A, Japan) was used to determine the surface morphology, and particle size and shape. The elemental compositions of the samples were determined by using energy dispersive x-rays (EDX) analyzer (Model JFC 1500 JEOL) connected with the SEM machine. The surface area, pore size and pore volume were determined by BET analyzer (Micromeritics Instrument Corp).

Synthesis of $\text{Zn}(\text{tmhd})_2$

Although $\text{Zn}(\text{tmhd})_2$ is available commercially but due to its simple synthesis process, we have synthesized it by the reaction of anhydrous $\text{Zn}(\text{OAc})_2$ with the 2,2,6,6-tetramethylheptane-3,5-dione (Htmhd) in well dried ethanol following a reported procedure [28]. In a typical experimental procedure adopted for the synthesis of $\text{Zn}(\text{tmhd})_2$, 13.761 g (75 mmol) of $\text{Zn}(\text{OAc})_2$ was dissolved in 100 mL of ethanol. The reaction flask was heated to reflux, and then 31.41 mL (150 mmol) of Htmhd dissolved in 150 mL of dried ethanol was added steadily. The stirring of the reaction mixture was continued for 2 hours while maintaining at 60°C . After cooling the reaction flask and maintaining at room temperature for certain time, the solvent was removed by rotary evaporator and a crystalline product amounting 10.64 g (yield: 80%) was obtained in the form of white powder. The resulting $\text{Zn}(\text{tmhd})_2$ complex was confirmed by IR, ^1H and ^{13}C NMR spectroscopy.

Preparation of ZnO in Acidic Medium

An appropriate amount of $\text{Zn}(\text{tmhd})_2$ was dissolved in 20 mL dried ethanol and acidified by adding 5mM HCl solution. The acid solution was added until a pH of 3 was achieved. After getting the desired pH of the reaction mixture, the refluxing was performed for 24 hours at 90°C . The precipitation of the solid residue was observed with that of reaction time. After completion of the sol gel process, the precipitate was separated from the supernatant by centrifugation at 6000 rpm for 60 minutes. The solid powder was thoroughly washed with ethanol and subsequently with distilled water to ensure complete

removal of the organics and anions. The cleaned powder was dried overnight (12 hours) in laboratory oven at 120°C. The resulting powder was divided into two parts and one part was sintered at 250°C while the other at 500°C in the muffle furnace. The sintering process lasted for four hours in each case.

Preparation of ZnO in Basic Medium

The basic process was the same as used for the synthesis of ZnO in acidic medium however HCl was replaced by NaOH to get the required basic medium for the reaction. In a typical process, the weighed amount of Zn(tmhd)₂ was dissolved in 20 mL dried ethanol and 5mM NaOH solution was added until the required pH of 9 was achieved. Subsequently, the reaction mixture was heated up to 90°C for 24 hours. The precipitation of white solid was observed with time. The solid residue was separated from the liquid by centrifuging at 6000 rpm for 60 minutes. The solid powder was washed thoroughly with ethanol and afterwards with distilled water to ensure complete removal of the organics and anions. The cleaned powder was dried overnight (12 hours) in laboratory oven at 120°C. The resulting powder was sintered at 250°C and 500°C for 4 hours in an open muffle furnace.

Results and Discussion

The Zn(tmhd)₂ was synthesized in laboratory instead of purchasing from the commercial sources i.e., by reacting anhydrous Zn(OAc)₂ with Htmhd following the reported procedure [28]. A small amount of NH₄OH was added to improve the product yield. The formation of compound Zn(tmhd)₂ was confirmed by comparing the IR, ¹H and ¹³C NMR spectra with the reported data [29].

The synthesized Zn(tmhd)₂ was hydrolyzed at pH 3, and sintered at 250°C (ZO1) and 550°C (ZO2). Likewise, the hydrolysis of Zn(tmhd)₂ was also carried out at pH 9, and sintered at 250°C (ZO3) and 550°C (ZO4). The microstructure (composition, shape and size of particles) of the ZnO nanomaterials were studied using different techniques. The diffractograms of samples are shown in Figure 1. The XRD patterns give peaks at 2θ of 31.76°, 34.41°, 36.24°, 47.51°, 56.58°, 62.85°, 66.35°, 67.92°, 68.98°, 72.67° and 76.93° matching well with the hexagonal (Wurtzite) crystal structure of ZnO (PDF: 01-079-2205) [30]. Although the ZnO nanomaterials have sufficient crystallinity, but the effect of pH and sintering temperature over the crystallite sizes are evident from the XRD patterns. The average crystallite sizes calculated using the well-known

Scherrer equation ($d = K\lambda/\beta\cos\theta$) are summarized in Table 1.

Table-1: Crystallite sizes of ZnO nanomaterials calculated using Scherrer equation.

Sample	Crystallite Size (nm)	Sample	Crystallite Size (nm)
ZO1	118 ± 4.57	ZO3	28 ± 2.69
ZO2	148 ± 3.81	ZO4	95 ± 3.14

As given in the Table 1, the crystallite size increases with increasing sintering temperature. The increase in grain (crystallite) size as a result of increasing sintering temperature is mainly due to the decrease in lattice strain by thermal activation and enhancement of crystallization of grain boundary structure [31, 32]. The effect of increasing pH over the crystallite size is contrary to the sintering temperature, as is evident from the patterns (Figure 1) and the data in Table 1. It has been seen mostly in the cases of oxides that the crystallite size decreases with increasing pH of the precipitating medium, without any known reasons.^[33-35] However, the presence of different ions in the precipitating medium influences the nucleation process. The fast transport of H⁺ ions in the acidic medium support the nucleation and the reverse is true for the Na⁺ ions present in the basic medium. The HO⁻ ions in the basic medium have a known effect over the nucleation process as these ions supersaturate the networks, slowing down the process of nucleation [36, 37]. The H⁺, Na⁺, and HO⁻ ions are present in the acidic and basic media used; therefore, the effect over crystallite size is evident.

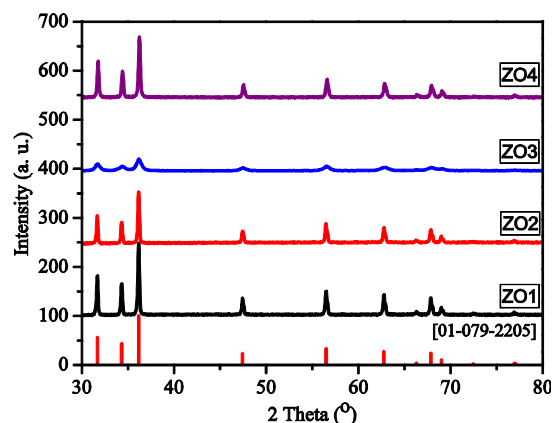


Fig. 1: XRD patterns of ZnO prepared at pH 3 followed by sintering at 250°C (ZO1) and 550°C (ZO2), and pH 9 followed by sintering at 250°C (ZO3) and 550°C (ZO4).

The elemental composition of the synthesized ZnO nanomaterials was determined by

EDX analysis coupled with SEM. The atom percent and mass composition of the samples are given in Table 1, while the EDX spectra are provided in supplementary materials. The oxygen contents of the samples decreases slightly upon increasing the sintering temperature which could be a result of the creation of oxygen vacancies due to the heating of the ZnO nanomaterials [38].

Table-2: Elemental composition determined by EDX and band gaps of ZnO nanomaterials.

Sample	Atom Percent		Mass Percent		Band gap (eV)
	Zn	O	Zn	O	
ZO1	49.74	50.26	80.17	19.83	2.15
ZO2	51.11	48.89	81.03	18.97	1.88
ZO3	51.04	48.96	80.99	19.01	2.09
ZO4	52.38	47.62	81.80	18.20	2.01

The UV-visible spectra of ZO1, ZO2, ZO3 and ZO4 are measured, and the band gap energies (E_g) are determined by plotting $(\alpha h\nu)^2$ as a function of $h\nu$ (Figure 2). The effect of pH and sintering temperature over E_g is evident from the calculated values (Table 2). The E_g decreased with the increasing sintering temperature in accordance with the literature [39, 40]. The decrease in E_g as a

function of increasing sintering temperature could be consequence of the generation of larger number of oxygen vacancies and the increasing particle size. We have seen in the preceding section that the concentration ratio of O/Zn decreases with the increasing sintering temperature owing to the generation of oxygen vacancies. The increasing number of oxygen vacancies contributes to the decreasing E_g . The SEM images (following section) have shown that the particle size increased significantly with the increasing sintering temperature. The increase in particle size is reflected in the decreasing values of E_g . Larger particle sizes in ZO3 and ZO4 have almost no significant effect on the value of E_g when compared to the same for ZO2, which have smaller particle size. The larger particle size in ZO3 and ZO4 is due to its synthesis at higher pH of 9 when compared to ZO2 which was prepared at pH 3. The E_g increases significantly with increasing pH of the medium [39, 40]. The decrease in E_g as a function of sintering temperature and the particle size is minimized by the increasing pH which has opposite effect upon the E_g as higher pH values favors larger particle sizes. It is also pertinent to mention here that the overall decrease in E_g compared to the bulk is significant.

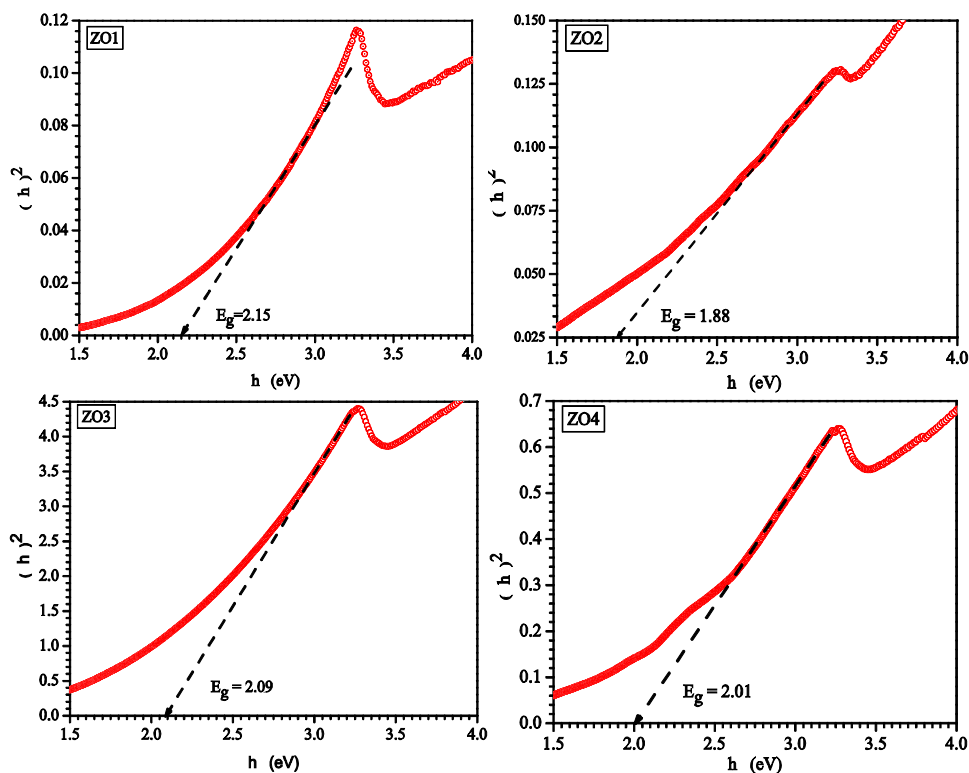


Fig. 2: Plots of calculated $(\alpha h\nu)^2$ as a function of $h\nu$ for determination of direct E_g of ZO1, ZO2, ZO3, and ZO4.

The effect of pH and sintering temperature over the particle size and shape of ZnO nanoparticles is evident from the SEM images recorded for ZO1, ZO2, ZO3, and ZO4 (Figure 3a-h). Rod like particles of diameters ranging from 0.2 – 0.5 μm and lengths of few microns were observed in the SEM images of ZO1 (Figure 3a, b). The particles were homogeneous in terms of morphology and uniformly distributed. The formation of elongated particles at pH 3 i.e., in acidic medium, corresponds to the fact that hydrolysis is the dominant reaction over the condensation in the sol gel process [41]. As the reaction proceeded new monomers added up to the growing chain thus leading to the formation of fibers. The fibers knit up together by the passive condensation reaction allowing the formation of rods. However, the ZnO nanoparticles prepared at pH 9 (ZO3) were spherical in shape and distributed homogeneously with uniform size of approximately 0.4 μm (Figure 3e, f). It is important to note that in basic medium, condensation reaction was dominant over the hydrolysis [41]. The hydroxyl groups attached to the metal center undergo condensation as soon as produced forming 3-D network, which led to the formation of spherical particles. The particles formed were well dispersed at the given sintering temperature in ZO1 (pH 3) and ZO3 (pH 9), irrespective of the pH of the media. Indeed, the acidic and basic media furnish plenty of charged ions (H^+ and HO^- , respectively) which adsorb at the surface of the particles. The similar charged particles have sufficient repulsive forces which are enough for retarding the coalescence and thus, keeping apart the particles as individual entities [42]. The sintering at 550°C transformed the ZnO into larger agglomerated particles, as evident from the SEM images given in Figure 3c, d (ZO2) and Figure 3g, h (ZO4). The typical morphologies of elongated rods and spherical particles in SEM images of ZO1 and ZO3 disappeared in ZO2 and ZO4 produced by heating of ZnO at 550°C. The pseudo one dimensional (1D) rods in ZO1 converted into pseudo two dimensional (2D) flat particles which were highly agglomerated. The appearance of hexagonal particle in the SEM image, shown in the inset of Figure 3c of ZO2 revealed the transformation from elongated rods to hexagonal particles. However, the temperature and/or the duration of sintering were not enough to obtain completely hexagonal particles. The particles of ZO2 were agglomerated having changed morphology and spaces in the form of channels among the particles. On the other hand, the sample (ZO4) prepared at pH 9 and sintered at 550°C has well developed hexagonal rod like particles, emerging from the base, where from other hexagonal rod like particles have also developed. The hexagonal rods have uniform diameters in the range of 0.8 – 1 μm . The shape of the hexagonal rods indicated that the growth was predominantly occurring along the *c*-axis of the unit cell. Similar rods of ZnO have been previously

prepared at elevated temperature (950°C) from ZnO powder upon substrates by thermal evaporation [43]. The particles are prone to agglomeration as a consequence of the increasing sintering temperature [44]. Therefore, irrespective of the pH, the particles of the samples ZO2 and ZO4 are agglomerated as shown in the SEM images (Figure 3c, d, g, h).

The ZnO nanoparticles were further investigated for their structural characteristics by FTIR spectroscopy (Figure 4a, b). The typical Zn – O stretching vibration peak appears at 431 cm^{-1} and 429 cm^{-1} in the IR spectra of ZO1 and ZO2, respectively [45, 46]. The relative red shift in the position of the band in IR spectrum of ZO2 is due to the comparatively larger particle size obtained as a result of increased sintering temperature [47]. The effect of sintering temperature over the band position of Zn – O bond is also observed in the IR spectrum of ZO4 showing peak at 433 cm^{-1} compared to the peak for the same bond in IR spectrum of ZO3 (438 cm^{-1}). However, the band for Zn – O bond in IR spectra of ZO3 and ZO4 appears at higher energies than those of ZO1 and ZO2. This can be correlated to the relatively smaller nanocrystallites structure obtained in the basic medium than those prepared in the acidic medium [47]. The decrease in nanocrystallites size range with increasing pH is also confirmed by the XRD analysis presented in the preceding paragraphs. Besides, other peaks appear in the range of 400 – 580 cm^{-1} corresponding to the IR spectra of ZnO materials reported in literature [48].

The BET analyses of the ZnO nanoparticles give the surface area, pore volume and size (Table 3). The BET surface areas of ZO1, ZO2, ZO3 and ZO4 are 14.26 m^2/g , 6.90 m^2/g , 68.95 m^2/g and 4.13 m^2/g , respectively. It is evident from the data that the surface area decreases with increasing sintering temperature. The decreases in BET surface area with the increase of sintering temperature from 250°C to 550°C is inevitable, because upon heating the particles agglomerate and increase in size, as shown by SEM, XRD, UV and IR analysis. The agglomeration and increase in size of particles are the factors responsible for reduction of the surface area [49]. The sample ZO3 has shown the highest BET surface area (68.95 m^2/g) in the series with comparatively bigger particles. The relatively larger surface area of ZO3 might be a result of the spherical shape of the ZnO nanoparticles. It has been previously observed that the spherical particles have a larger surface area than the rod like particles [50]. The ZO1 and ZO2 have elongated and distorted elongated while the ZO4 have hexagonal rod like particles, respectively. However, the ZO3 have spherical particles due to which the sample has larger surface area than the rest of the members of the series.

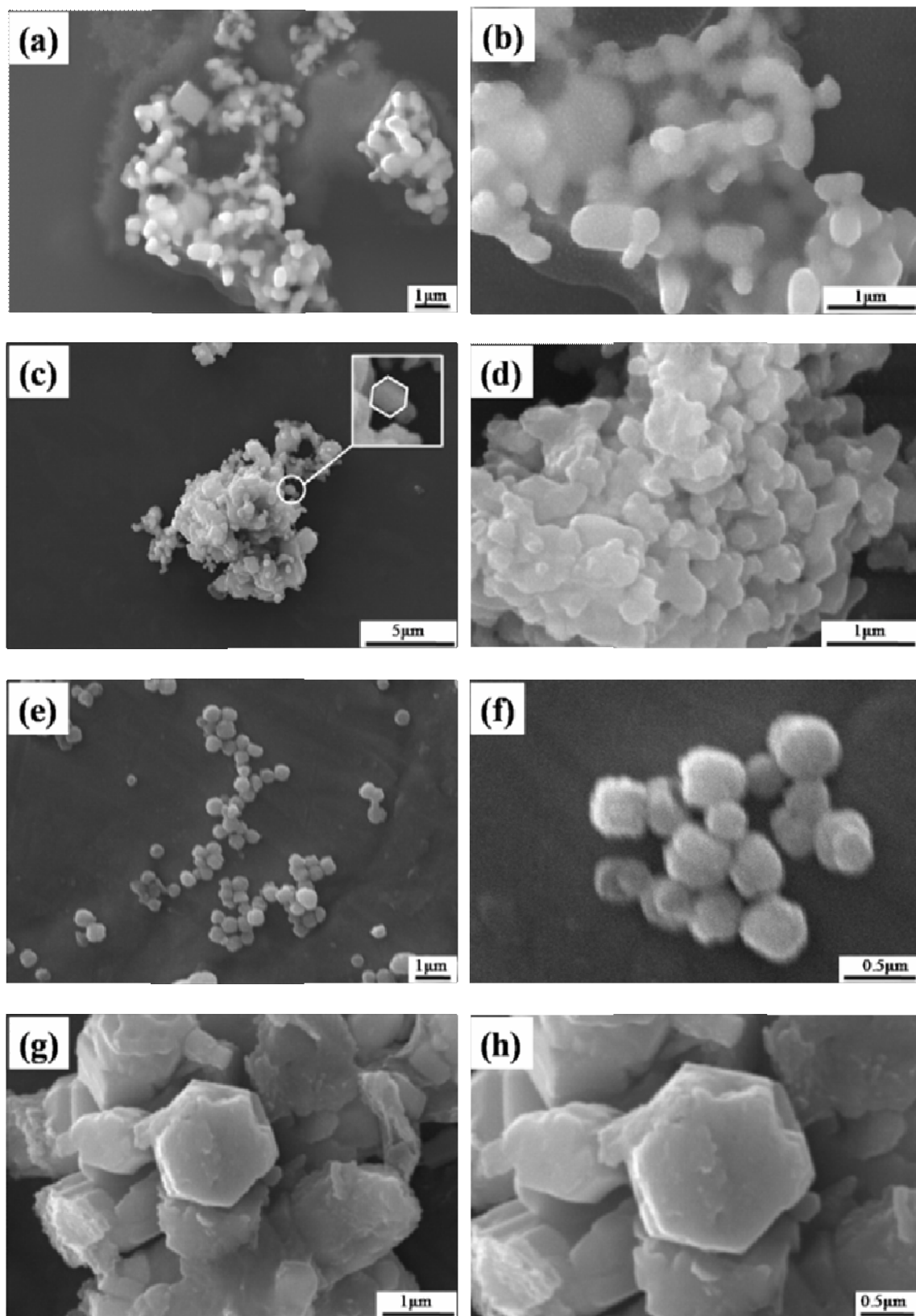


Fig. 3: SEM images of ZOI (a, b), ZO2 (c, d), ZO3 (e, f), and ZO4 (g, h).

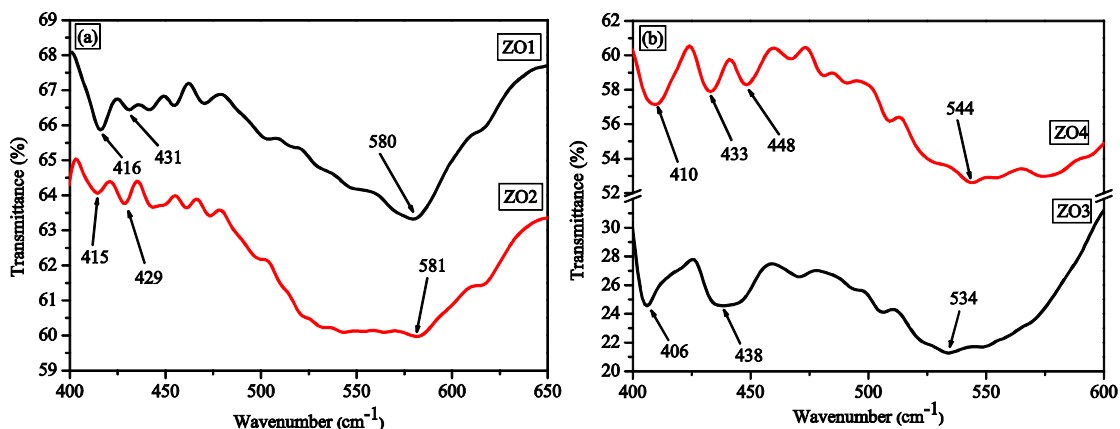


Fig. 4: IR spectra of ZO1 and ZO2 (a), and ZO3 and ZO4 (b).

Table-3: Surface area, pore volume and size determined by the BET technique.

Sample	BET Surface Areas (m ² /g)	Pore Volume (cm ³ /g)	Pore Size (Å)
ZO1	14.26	4.4 × 10 ⁻³	12.27
ZO2	06.90	2.9 × 10 ⁻³	16.55
ZO3	68.95	2.8 × 10 ⁻²	16.40
ZO4	04.13	1.9 × 10 ⁻³	18.02

The β -diketone is responsible for the formation of uniform size and shape particles in the form of cylindrical rods in ZO1 and spheres in ZO3. The ligand is furnished to the solution as stable molecular organic entity which has strong anchoring groups. These groups help in attaching of β -diketone to the ZnO particles formed by the Ostwald's ripening and/or aggregation, and thus, hindering their further coagulation [51]. The β -diketone molecules have significant effect over the shape of particles and acts as template in directing the structure of the very initial ZnO particles. However, the presence of H⁺ and HO⁻ ions as particle size controlling species could not be rolled out because these ions as adsorbed charges upon the ZnO particles are responsible for the electrostatic repulsion among the particles [42]. The repulsive forces hinder excessive coagulation and aggregation of the particles into irregular bulks. Spherical nanoparticles of ZnO have been obtained by sol gel method in previous attempts but on the expenses of addition of external stabilizing agent [52]. Alike of precursor, Zn(acac)₂, gave hollow ZnO nanoparticles upon hydrolysis at elevated pH [25]. This indicates that the formation of ZnO spherical particles may be specifically due to the precursor used in this study. The transformation of cylindrical and spherical ZnO nanoparticles to

hexagonal shaped particles upon sintering could be corresponded to the orientation of particles into stable hexagons which grow hierarchical with (increasing) temperature. The role of H⁺ and HO⁻ in hindering the agglomeration of ZnO nanoparticles of ZO1 and ZO3 is also evident from the fact that the particles of ZO2 and ZO4 are relatively more agglomerated. In fact, heating eliminates the adsorbed H⁺ and HO⁻ ions, responsible for the electrostatic repulsive forces among the particles, and as a consequence rate of the agglomeration of particles increases.

Conclusions

ZnO nanoparticles are prepared by simple hydrolysis of a metal organic molecular precursor. The crystal structure, chemical composition, morphology and electronic properties of the resulting ZnO nanoparticles are dependent upon the nature of the reaction media, pH and sintering temperature. All the samples crystallized in Wurtzite (hexagonal) crystal structure. The particles sintered at 250°C after the preparation at pH 3 and pH 9 has elongated rod like and spherical shapes respectively. However, the morphologies of ZnO nanoparticles prepared at pH 3 and pH 9 while sintered at 550°C are completely different. Hexagonal rod shaped particles formed in the sample prepared at pH 9 and heated at 550°C. The hexagons formation started in the sample obtained at pH 3 upon heating up to 500°C. However, the formation process seems to be incomplete.

Acknowledgements

The research work was supported by the Higher Education Commission (HEC) of Pakistan. Therefore, the authors are grateful for the financial

support provided by the HEC through the project PM-IPFP/HRD/HEC/2011/374.

References

1. R. Baron, F. W. Campbell, I. Streeter, L. Xiao and R. G. Compton, Facile Method for the Construction of Random Nanoparticle Arrays on a Carbon Support for the Development of Well defined Catalytic Surfaces, *Int. J. Electrochem. Sci.*, **3**, 556 (2008).
2. A. B. Moghaddam, M. Kazemzad, M. R. Nabid and H. H. Dabaghi, Improved Voltammograms of Hydrocaffeic Acid on the Single-Walled Carbon Nanotube/Graphite-Film Surfaces, *Int. J. Electrochem. Sci.*, **3**, 291 (2008).
3. D. J. Milliron, S. M. Hughes, Y. Cui, L. Manna, J. Li, L.-W. Wang and A. P. Alivisatos, Colloidal Nanocrystal Heterostructures with Linear and Branched Topology, *Nature*, **430**, 190 (2004).
4. C. M. Lieber, One-Dimensional Nanostructures: Chemistry, Physics & Applications, *Solid State Commun.*, **107**, 607 (1998).
5. D. C. Look, Recent Advances in ZnO Materials and Devices, *Mater. Sci. Eng. B*, **80**, 383 (2001).
6. R. Bacsa, A. Sienkiewicz, K. Pierzchała, J. Dexpert-Ghys, L. Forro and P. Serp, CVD Synthesis of Shape and Size Controlled ZnO Nanoparticles for Application as UV Filters, *ECS Transactions*, **25**, 1177 (2009).
7. J. A. Rodriguez, T. Jirsak, J. Dvorak, S. Sambasivan and D. J. Fischer, Reaction of NO₂ with Zn and ZnO: Photoemission, XANES, and Density Functional Studies on the Formation of NO₃, *J. Phys. Chem. B*, **104**, 319 (2000).
8. W.-C. Shin and M.-S. Wu, Growth of ZnO Films on GaAs Substrates with a SiO₂ Buffer Layer by RF Planar Magnetron Sputtering for Surface Acoustic Wave Applications, *J. Cryst. Growth*, **137**, 319 (1994).
9. H. M. Huang, S. Mao, H. Feick, H. Yan, Y. Wu, H. Kind, E. Weber, R. Russo and P. D. Yang, Room-Temperature Ultraviolet Nanowire Nanolasers, *Science*, **292**, 1897 (2001).
10. N. F. Cooray, K. Kushiya, A. Fujimaki, D. Okumura, M. Sato, M. Ooshita and O. Yamase, Optimization of Al-doped ZnO Window Layers for Large-Area Cu(InGa)Se₂-Based Modules by RF/DC/DC Multiple Magnetron Sputtering, *Jpn. J. Appl. Phys.*, **38**, 6213 (1999).
11. R. Paneva and D. Gotchev, Non-Linear Vibration Behavior of Thin Multilayer Diaphragms, *Sens. Actuat. A: Phys.*, **72**, 79 (1999).
12. E. Topoglidis, A. E. G. Cass, B. Oregan and J. R. Durrant, Immobilisation and Bioelectrochemistry of Proteins on Nanoporous TiO₂ and ZnO Films, *J. Electroanal. Chem.*, **517**, 20 (2001).
13. L. Gao, Q. Li, W. L. Luan, H. Kawaoka, T. Sekino, and K. Niihara, Preparation and Electric Properties of Dense Nanocrystalline Zinc Oxide Ceramics, *J. Am. Ceram. Soc.*, **85**, 1016 (2002).
14. C. X. Xu and X. W. Sun, Field Emission From Zinc Oxide Nanopins, *Appl. Phys. Lett.*, **83**, 3806 (2003).
15. P. X. Gao, Y. Ding, W. Mai, W. L. Hughes, C. S. Lao and Z. L. Wang, Conversion of Zinc Oxide Nanobelts into Superlattice-Structured Nanohelices, *Science*, **309**, 1700 (2005).
16. A. B. Moghaddam, T. Nazari, J. Badraghi and M. Kazemzad, Synthesis of ZnO Nanoparticles and Electrodeposition of Polypyrrole/ZnO Nanocomposite Film, *Int. J. Electrochem. Sci.*, **4**, 247 (2009).
17. Y. H. Huang, Y. Zhang, X. M. Zhang, J. Liu, J. He, and Q. L. Liao, Structures, Growth Mechanisms and Properties of ZnO Nanomaterials Fabricated by Zinc Powder Evaporation, *Nanoscience*, **11**, 265 (2006).
18. L. Znaidi, Sol-gel-Deposited ZnO Thin Films: A review, *Materials Science and Engineering B*, **174**, 18 (2010).
19. M. Guglielmi and G. Carturan, Precursors for Sol-Gel Preparations, *J. Non-Cryst. Solids*, **100**, 16 (1988).
20. L. Armelao, M. Fabrizio, S. Gialanella and F. Zordan, Sol-Gel Synthesis and Characterisation of ZnO-Based Nanosystems, *Thin Solid Films*, **394**, 89 (2001).
21. M. Ohyama, H. Kozuka and T. Yoko, Sol-Gel Preparation of ZnO Films with Extremely Preferred Orientation Along (002) Plane from Zinc Acetate Solution, *Thin Solid Films*, **306**, 78 (1997).
22. S.-Y. Chu, T.-M. Yan and S.-L. Chen, Characteristics of Sol-Gel Synthesis of ZnO-Based Powders, *J. Mater. Sci. Lett.*, **19**, 349 (2000).
23. D. W. Bahnemann, C. Kormann and M. R. Hoffmann, Preparation and Characterization of Quantum Size Zinc Oxide: A Detailed Spectroscopic Study, *J. Phys. Chem.*, **91**, 3789 (1987).
24. M. Tiitta and L. Niinisto, Volatile Metal β-Diketonates: ALE and CVD precursors for Electroluminescent Device Thin Films, *Chem. Vap. Deposition*, **3**, 167 (1997).
25. S. Musić, A. Šarić, Formation of Hollow ZnO Particles by Simple Hydrolysis of Zinc Acetylacetonate, *Ceram. Int.*, **38**, 6047 (2012).
26. L. V. Saraf, M. H. Engelhard, C. M. Wang, A. S. Lea, D. E. McCready, V. Shutthanandan, D. R. Baer and S. A. Chambers, Metalorganic Chemical Vapor Deposition of Carbon-Free ZnO using the bis(2,2,6,6-tetramethyl-3,5-heptanedionato)Zinc Precursor, *J. Mater. Res.*, **22**, 1230 (2007).
27. A. Short, L. Jewell, S. Doshay, C. Church, T. Keiber, F. Bridges, S. Carter and G. Alers, Atomic Layer Deposition of Zinc Sulfide with Zn(TMHD)₂, *J. Vac. Sci. Technol. A*, **31**, 01A138 (2013).
28. T. Zhang, H. Gu, F. Ding, F. Qu and S. Dai, Synthesis, Characterization, and Thermostability of bis(2,2,6,6-tetramethyl-3,5-

- heptanedionato)Copper(II), *Rare Metals*, **13**, 343 (2012).
29. M. Shirodker, V. Borker, C. Nather, W. Bensch and K. S. Rane, Synthesis and Structure of tris(acetylacetonato) Aluminum(III), *Indian J. Chem.*, **49**, 1607 (2010).
 30. G. He, B. Huang, S. Wu, J. Li and Q.-H. Wu, Structure Morphologies and Luminescence Properties of ZnO Nanomaterials Synthesized by an Acidic Solution Process, *J. Phys. D: Appl. Phys.*, **42**, 215401 (2009).
 31. T. P. Raming, A. J. A. Winnubst, C. M. Van Kats and A. P. Philipse, The Synthesis and Magnetic Properties of Nanosized Hematite (α -Fe₂O₃) Particles, *J. Colloid Interface Sci.*, **249**, 346 (2002).
 32. B. G. Toksha, E. S. Shirsath, S. M. Patange and K. M. Jadhav, Structural Investigations and Magnetic Properties of Cobalt Ferrite Nanoparticles Prepared by Sol-Gel Auto Combustion Method, *Solid State Commun.*, **147**, 479 (2008).
 33. M. Srivastava, A. K. Ojha, S. Chaubey, P. K. Sharma and A. C. Pandey, Influence of pH on Structural Morphology and Magnetic Properties of Ordered Phase Cobalt Doped Lithium Ferrites Nanoparticles Synthesized by Sol-Gel Method, *Mater. Sci. Eng. B*, **175**, 14 (2010).
 34. K. H. Wu, W. C. Huang, G. P. Wang and T. R. Wu, Effect of pH on the Magnetic and Dielectric Properties of SiO₂/NiZn Ferrite Nanocomposites, *Mater. Res. Bull.*, **40**, 1822 (2005).
 35. Z. Wu, W. Zhou, W. Jin and N. Xu, Effect of pH on Synthesis and Properties of Perovskite Oxide via a Citrate Process, *AIChE J.*, **52**, 769 (2006).
 36. K. S. A. Kumar and R. N. Bhowmik, Micro-Structural Characterization and Magnetic Study of Ni_{1.5}Fe_{1.5}O₄ Ferrite Synthesized Through Coprecipitation Route at Different pH Values, *Mater. Chem. Phys.*, **146**, 159 (2014).
 37. J. de Vicente, A. V. Delgado, R. C. Plaza, J. D. G. Duran and F. G. Caballero, Stability of Cobalt Ferrite Colloidal Particles. Effect of pH and Applied Magnetic Fields, *Langmuir*, **16**, 7954 (2000).
 38. A. Sedky, T. A. El-Brollosy and S. B. Mohamed, Correlation Between Sintering Temperature and Properties of ZnO Ceramic Varistors, *Journal of Physics and Chemistry of Solids*, **73**, 505 (2012).
 39. J. Uchil and M. Pattabi, Preparation and Characterization of CdS Nanoparticles in an Aqueous Medium Using Chicken Egg Membrane, *Journal of New Materials for Electrochemical Systems*, **8**, 109 (2005).
 40. S. F. Shayesteh, S. Kolahi and Y. Azizian-Kalandarragh, Effect of pH on the Structural and Optical Properties of ZnS Nanoparticles Embedded in PVA Matrix, *Indian J. Pure Appl. Phys.*, **51**, 780 (2013).
 41. K. D. Keefer, in *Silicon Based Polymer Science: A Comprehensive Resource*, (Eds.: J. M. Zeigler, F. W. G. Fearon), American Chemical Society, Washington DC, p. 227 (1990).
 42. D. Bahnemann, A. Henglein and L. Spanhel, Detection of the Intermediates of Colloidal TiO₂-Catalysed Photoreactions, *Faraday Discuss. Chem. Soc.*, **78**, 151 (1984).
 43. Z. Y. Wu, I. J. Chen, Y. F. Lin, S. P. Chiu, F. R. Chen, J. J. Kai, J. J. Lin and W. B. Jian, Cross-Sectional Shape Modulation of Physical Properties in ZnO and Zn_{1-x}Co_xO Nanowires, *New J. Phys.*, **10**, 033017 (2008).
 44. J. Ye, R. Zhou, C. Zheng, Q. Sun, Y. Lv, C. Li and X. Hou, Size-Controllable Synthesis of Spherical ZnO Nanoparticles: Size- and Concentration-Dependent Resonant Light Scattering, *Microchem. J.*, **100**, 61 (2012).
 45. G. Xiong, U. Pal, J. G. Serrano, K. B. Ucer and R. T. Williams, Photoluminescence and FTIR Study of ZnO Nanoparticles: the Impurity and Defect Perspective, *Phys. Stat. Sol.*, **3**, 3577 (2006).
 46. A. Becheri, M. Duerr, P. L. Nostro and P. Baglioni, Synthesis and Characterization of Zinc Oxide Nanoparticles: Application to Textiles as UV-Absorbers, *J. Nanopart. Res.*, **10**, 679 (2008).
 47. S. Dutta and B. N. Ganguly, Characterization of ZnO Nanoparticles Grown in Presence of Folic Acid Template, *J. Nanobiotechnology*, **10**, 29 (2012).
 48. K. Segala, R. L. Dutra, C. V. Franco, A. S. Pereira and T. Trindade, *In situ* and *Ex Situ* Preparations of ZnO/poly- $\{trans-[RuCl_2(vpy)_4]/styrene\}$ Nanocomposites, *J. Braz. Chem. Soc.*, **21**, 1986 (2010).
 49. X. Zhang, J. Qin, Y. Xue, P. Yu, B. Zhang, L. Wang and R. Liu, Effect of Aspect Ratio and Surface Defects on the Photocatalytic Activity of ZnO Nanorods, *Sci. Rep.*, **4**, 4596 (2014).
 50. X. Huang, X. Teng, D. Chen, F. Tang and J. He, The Effect of the Shape of Mesoporous Silica Nanoparticles on Cellular Uptake and Cell Function, *Biomaterials*, **31**, 438 (2010).
 51. L. Znaidi, G. J. A. A. SolerIllia, S. Benyahia, C. Sanchez and A. V. Kanaev, Oriented ZnO Thin Films Synthesis by Sol-Gel Process for Laser Application, *Thin Solid Films*, **428**, 257 (2003).
 52. C.-H. Hsieh, Spherical Zinc Oxide Nano Particles from Zinc Acetate in the Precipitation Method, *J. Chin. Chem. Soc.*, **54**, 31 (2007).